Systems analysis of the glycoside hydrolase family 18 enzymes from *Cellvibrio japonicus* characterizes essential chitin degradation functions

Received for publication, November 7, 2017, and in revised form, January 10, 2018 Published, Papers in Press, January 24, 2018, DOI 10.1074/jbc.RA117.000849

Estela C. Monge[‡], Tina R. Tuveng[§], Gustav Vaaje-Kolstad[§], Vincent G. H. Eijsink[§], and Jeffrey G. Gardner[‡1]

From the [‡]Department of Biological Sciences, University of Maryland, Baltimore County, Baltimore, Maryland 21250 and the [§]Faculty of Chemistry, Biotechnology and Food Science, Norwegian University of Life Sciences, 1430 Ås, Norway

Edited by Gerald W. Hart

Understanding the strategies used by bacteria to degrade polysaccharides constitutes an invaluable tool for biotechnological applications. Bacteria are major mediators of polysaccharide degradation in nature; however, the complex mechanisms used to detect, degrade, and consume these substrates are not well-understood, especially for recalcitrant polysaccharides such as chitin. It has been previously shown that the model bacterial saprophyte *Cellvibrio japonicus* is able to catabolize chitin, but little is known about the enzymatic machinery underlying this capability. Previous analyses of the *C. japonicus* genome and proteome indicated the presence of four glycoside hydrolase family 18 (GH18) enzymes, and studies of the proteome indicated that all are involved in chitin utilization. Using a combination of *in vitro* and *in vivo* approaches, we have studied the roles of these four chitinases in chitin bioconversion. Genetic analyses showed that only the *chi18D* gene product is essential for the degradation of chitin substrates. Biochemical characterization of the four enzymes showed functional differences and synergistic effects during chitin degradation, indicating nonredundant roles in the cell. Transcriptomic studies revealed complex regulation of the chitin degradation machinery of *C. japonicus* and confirmed the importance of *Cj*Chi18D and *Cj*LPMO10A, a previously characterized chitin-active enzyme. With this systems biology approach, we deciphered the physiological relevance of the glycoside hydrolase family 18 enzymes for chitin degradation in *C. japonicus*, and the combination of *in vitro* and *in vivo* approaches provided a comprehensive understanding of the initial stages of chitin degradation by this bacterium.

Chitin, a linear polymer of $\beta(1-4)$-linked *N*-acetylglucosamine, is the second most abundant polysaccharide on earth after cellulose and a major source of fixed carbon and nitrogen, especially in the oceans (1). The rate of chitin degradation has been calculated to match the rate of synthesis, resulting in little net accumulation of chitin in the environment, suggesting that the microorganisms that derive nutrition from this polysaccharide are able to degrade it with high efficiency (2). Moreover, chitin is increasingly being recognized as an important feedstock for the production of renewable chemicals, and chitooligosaccharides are being investigated for several biomedical applications (3–6). The strategies used by microbes for efficient chitin bioconversion are gaining interest, because current chemical methods used for the industrial processing of chitin are inefficient and wasteful (7, 8). Therefore, the combination of environmental importance and industrial/medical relevance has renewed interest in the bioconversion of chitin (9, 10).

Depolymerization of chitin-rich substrates has been studied predominately from biochemical and structural perspectives, and as a consequence there is considerable understanding on certain mechanistic aspects of enzymatic degradation (11). Chitin deconstruction shares many features with cellulose degradation, which is not surprising given that chitin has a crystalline structure similar to that of cellulose and differs chemically via an *N*-acetyl substitution at the C2 carbon (12). Specifically, chitin depolymerization is achieved through a concerted effort of endo- and exo-acting enzymes to reduce polymer length to short oligosaccharides that are then converted to *N*-acetylglucosamine monomers by hexosaminidases for entry into cellular metabolism (Fig. 1) (6). Additionally, the action of lytic polysaccharide monooxygenases (LPMO)[2] in aerobic microbes promotes chitin degradation by acting on crystalline regions of the substrate (13–15).

Physiological and genetic aspects of chitin degradation, especially for terrestrial bacteria, are not well-characterized. One reason for this lack of knowledge is the multiplicity of chitinolytic enzymes in many, but not all, chitin-degrading bacteria, which makes functional analysis of the individual enzymes challenging. Although several model organisms have been used to study chitin degradation (16–18), one that is emerging as a powerful model, because of the available systems biology tools,

This work was supported by start-up funds (to J. G. G.); by Grant 2-R25-GM55036 from the Meyerhoff Graduate Fellows Program under the NIGMS, National Institutes of Health Initiative for Maximizing Student Development, by Chemistry and Biology Interface Program Grant T32-GM066706 (to E. C. M.); and Grant 221576 from the Research Council of Norway (to T. R. T., G. V. K., and V. G. H. E.). The authors declare that they have no conflicts of interest with the contents of this article. The content is solely the responsibility of the authors and does not necessarily represent the official views of the National Institutes of Health.

This article contains references, Tables S1–S6, and Figs. S1–S7.

[1] To whom correspondence should be addressed: Dept. of Biological Sciences, University of Maryland, Baltimore County, Baltimore, MD 21250. Tel.: 410-455-3613; Fax: 410-455-3875; E-mail: jgardner@umbc.edu.

[2] The abbreviations used are: LPMO, lytic polysaccharide monooxygenase; GH, glycoside hydrolase family; CAZyme, carbohydrate active enzyme; CBM, carbohydrate-binding module; Glc, glucose; OD, optical density; SPII, signal peptidase II; BisTris, 2-[bis(2-hydroxyethyl)amino]-2-(hydroxymethyl) propane-1,3-diol.

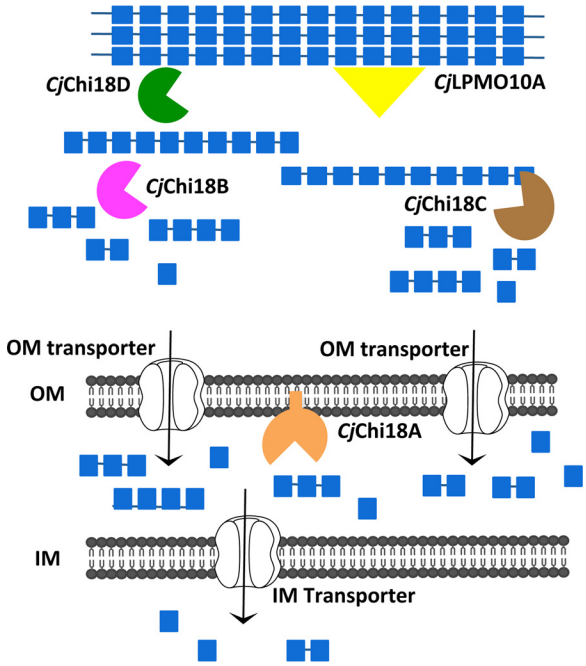

Figure 1. Proposed model for chitin utilization in *C. japonicus*. *Cj*Chi18D (*green*) and *Cj*LPMO10A (*yellow*) work together to disrupt the crystalline structure of chitin and degrade less accessible chitin fibers, whereas *Cj*Chi18B (*magenta*) and *Cj*Chi18C (*brown*) are acting on the more accessible chitin fibers to produce chito-oligosaccharides, which are taken up into the periplasm space. *Cj*Chi18A (*orange*) generates GlcNAc, and this lipoprotein may be acting in the periplasmic space (as shown here) or may be located on the outer side of the outer membrane and act outside the cell. *IM*, inner membrane; *OM*, outer membrane. Transporter icons (*white*) and phospholipids (*gray*) are adapted from Servier Medical Art under a Creative Commons Attribution 3.0 Unported License (https://creativecommons.org/licenses/by/3.0/).

is the saprophytic Gram-negative bacterium *Cellvibrio japonicus* (19, 20). This bacterium is a potent chitin degrader (13) and has a suite of nine genes encoding enzymes with predicted functions in chitin degradation (21). Specifically, the *C. japonicus* genome is predicted to encode four chitinases from the glycoside hydrolase family 18 (GH18), one GH19 chitinase, two hexosaminidases (GH20), one chitosanase (GH46), and one chitin-specific LPMO (auxiliary activity, AA10) (21). Secretome analysis (22) has shown that the four GH18s, and to a much lesser extent the GH19, are abundant during growth on chitin. Generally, the GH18s and LPMOs are considered key enzymes for bioconversion of crystalline chitin. The physiological role of GH19 enzymes in chitin degradation is less clear (23, 24).

The possession of large numbers of carbohydrate active enzymes (CAZymes) (25) is a hallmark feature of *C. japonicus*. There is increasing evidence that the CAZymes of *C. japonicus* that belong to the same GH family are not functionally redundant but have unique physiological functions (14, 26). In the current study, the physiological roles of the four *C. japonicus* GH18 chitinases were determined focusing on the initial stages of chitin degradation. Sequence analysis indicates that *Cj*Chi18B *Cj*Chi18C and *Cj*Chi18D are secreted enzymes containing at least one chitin-specific carbohydrate-binding module (CBM), whereas *Cj*Chi18A is a single domain protein that likely is membrane-anchored (Fig. 2). Through RNAseq analysis, we determined that these four chitinases were highly up-regulated while chitin was being used as the sole carbon source. Combinatorial mutational analyses determined that only the *chi18D* gene product is essential for chitin degradation. Biochemical characterization of the catalytic domains of these four GH18 chitinases indicated that *Cj*Chi18D is substantially more active toward insoluble chitin than the other GH18 chitinases, underpinning its importance in chitin degradation. The functional insights into the initial stages of chitin degradation by saprophytic bacteria that are provided in this study have the potential to accelerate the development of industrial chitin bioconversion strategies.

Results

CjChi18D is essential for the degradation of α-chitin

According to previous sequence analysis (21), *C. japonicus* possesses four GH18 chitinases (*Cj*Chi18A, *Cj*Chi18B, *Cj*Chi18C, and *Cj*Chi18D). A recent proteomic study (22) detected the four enzymes in the secretome of *C. japonicus* growing on α- and β-chitin, which suggested the importance of these enzymes for efficient chitin degradation. To elucidate the physiological relevance of these enzymes, we generated a suite of GH18 deletion mutants and assessed their fitness on insoluble chitin substrates, including an environmentally relevant substrate, crab shell.

Wildtype and GH18 deletion mutant strains all grew well in defined media with either glucose (Glc) or GlcNAc as the sole source of carbon (Fig. S1). A Δ*gsp* mutant, which lacks the entire 9.4 kb *gsp* operon encoding the type II secretion system that is needed for secretion of most enzymes, was also able to grow on these monosaccharides, as previously demonstrated (13, 27). When the GH18 single deletion mutants were grown using insoluble α-chitin or crab shell as the sole carbon source, distinct phenotypes emerged (Fig. 3). When α-chitin was the sole source of carbon, the Δ*chi18D* mutant was unable to grow. The other three single deletion strains (Δ*chi18A*, Δ*chi18B*, and Δ*chi18C*) all had similar growth rates and maximum optical densities (OD) as the wildtype (Table S1*A*). Interestingly, the Δ*chi18B* and Δ*chi18C* single mutant strains had more protracted lag phases than the wildtype strain when using α-chitin as carbon source (Fig. 3*A*). When using crab shells as the only source of carbon, the Δ*chi18D* mutant was unable to grow, whereas the single mutants of Δ*chi18A*, Δ*chi18B*, and Δ*chi18C* displayed growth similar to wildtype (Fig. 3*C* and Table S1*B*).

To test for functional redundancies between the GH18 chitinases, we generated all combinations of double deletion mutants and then assessed growth using α-chitin or crab shells as the sole carbon source. The double mutant Δ*chi18B* Δ*chi18C* resulted in a slower growth rate and a longer lag phase when grown on α-chitin in comparison to either of the single deletion mutants or the wildtype (Fig. 3*B*). The growth rate of the Δ*chi18B* Δ*chi18C* double mutant was reduced 37% compared with wildtype (Table S1*A*). The Δ*chi18A* Δ*chi18B* double mutant grew like the Δ*chi18B* single mutant, whereas the Δ*chi18A* Δ*chi18C* double mutant grew like the Δ*chi18C* single mutant. The Δ*chi18A* Δ*chi18B* Δ*chi18C* triple mutant recapitulated the growth defect observed in the Δ*chi18B* Δ*chi18C* double mutant in terms of the growth rate, lag phase, and the maximum OD (Fig. 3*B* and Table S1*A*). These results suggest that the *chi18B* and *chi18C* gene products have non-redundant

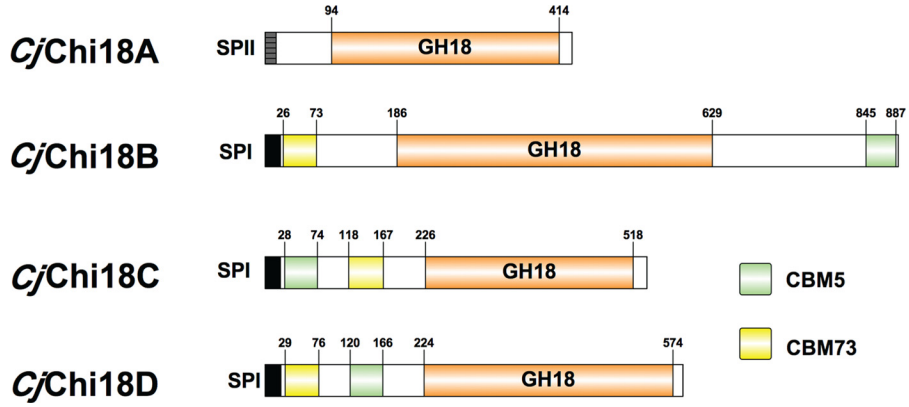

Figure 2. Diverse architecture of the family GH18 chitinases of *C. japonicus*. CAZy domain representation of the family GH18 chitinases of *C. japonicus* is shown. The indicated domains are as follows: *GH18*, family GH18 catalytic domain; *CBM5*, chitin-binding domain; *CBM73*, chitin-binding domain; *SPI*, signal peptide, type I; *SPII*, signal peptide, type II. This image was generated using IBS Illustrator (65).

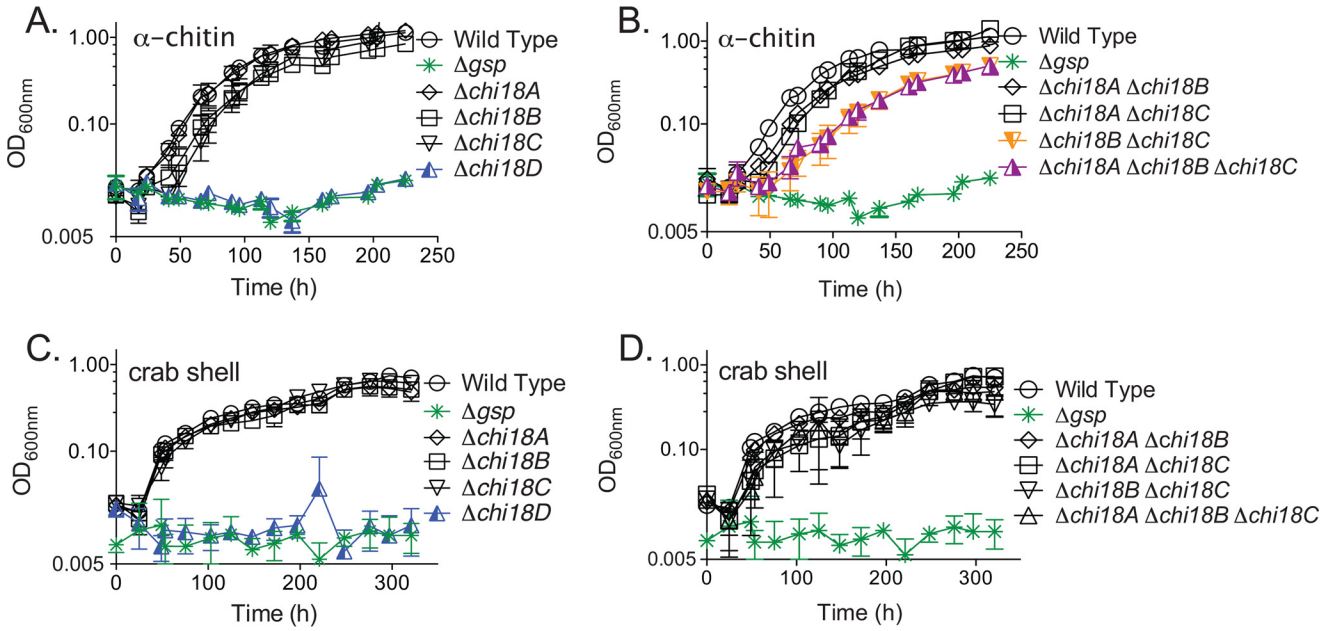

Figure 3. Growth of *C. japonicus* mutants on chitin. Deletion mutants were grown using MOPS minimal medium supplemented with 0.25% α-chitin (*A* and *B*) or 4% crab shell (*C* and *D*). *A* and *C* show single mutants; *B* and *D* show multiple mutants. All experiments were performed in biological triplicate; *error bars* represent standard deviations but in many cases are too small to be observed. These growth experiments were performed simultaneously but are separated into multiple panels for clarity. As a consequence, the same control strains (wildtype and Δ*gsp*) are repeated in each panel for a given substrate.

functions during degradation of α-chitin, whereas the *chi18A* gene product does not play a rate-limiting role.

Interestingly, the double mutants exhibited wildtype-like phenotypes when grown using crab shells as the sole carbon source (Fig. 3*D*). The growth rates of the Δ*chi18B* and Δ*chi18C* single mutants and the Δ*chi18B* Δ*chi18C* double mutant were similar to the wildtype strain when grown using crab shells. For all tested strains, the growth rates when using crab shells as the sole carbon source were substantially reduced compared with α-chitin. The results of experiments using β-chitin (Fig. S2) were very similar to the results obtained with α-chitin.

CjChi18D is a potent secreted chitinase

Sequence alignment of the catalytic domains of the four chitinase showed large sequence variation. *Cj*Chi18A and *Cj*Chi18D share higher sequence identity (32%), whereas *Cj*Chi18C and *Cj*Chi18D showed the lowest identity (19%), as determined by BLAST alignment (28). As predicted by LipoP (29) and SignalP (30) software tools, all four of the *C. japonicus* GH18 chitinases have a signal sequence; however, *Cj*Chi18A has a SPaseII-cleaveable sequence and is predicted to be an outer membrane associated lipoprotein. The *Cj*Chi18B, *Cj*Chi18C, and *Cj*Chi18D enzymes have a SPaseI-cleaved sequence (29) and are predicted to be secreted. The domain structure of the four GH18 chitinases is summarized in Fig. 2. The LipoP/SignalP software predictions are in agreement with a proteomics study that showed the occurrence of all four GH18 chitinases in the secretome (22).

To further assess the contribution of individual GH18 enzymes as effectors of chitin degradation, we used our suite of GH18 mutants to assess secreted activity using colloidal chitin plate assays (Fig. 4 and Table S2). A wildtype strain generated a robust zone of clearing, whereas a Δ*gsp* secretion-deficient mutant generated no zone of clearing. We observed a similarly

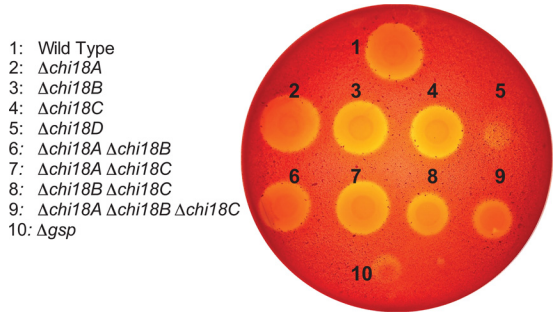

Figure 4. Chitinase secretion of *C. japonicus* GH18 mutants. Strains were grown on a plate that contained MOPS with 1.5% agar, 2% colloidal chitin, and 0.2% glucose. After incubation at 30 °C for 5 days, the plates were stained with Congo red. This experiment was conducted in biological triplicate, and quantification of the clearing zones is shown in Table S2.

striking phenotype with the Δ*chi18D* single mutant strain, which also generated no zone of clearing. The remaining GH18 single mutants displayed approximately wildtype zones of clearing. Interestingly, relative to the wildtype, the Δ*chi18B* Δ*chi18C* double mutant showed a clear reduction in the size of the clearing zone. The Δ*chi18A* Δ*chi18B* Δ*chi18C* triple mutant displayed a zone of clearing similar to the Δ*chi18B* Δ*chi18C* double mutant. The reduced chitin-degrading capacities of the Δ*chi18B* Δ*chi18C* double mutant and the Δ*chi18A* Δ*chi18B* Δ*chi18C* triple mutant are in agreement with the observed growth defects of these strains when grown on α-chitin.

The GH18 chitinases have different activities toward chitin and $(GlcNAc)_6$

To further investigate the features of the four GH18 chitinases, they were cloned, expressed, and purified for biochemical characterization. Despite substantial efforts, soluble full-length multidomain *Cj*Chi18B, *Cj*Chi18C, and *Cj*Chi18D proteins could not be obtained. Therefore comparative biochemical analysis was conducted with overexpressed catalytic domains. All four chitinases were able to degrade α-chitin, although with greatly varying efficiency, but were clearly highest for *Cj*Chi18D (Fig. 5). As expected (31), versions of *Cj*Chi18B and *Cj*Chi18D containing their CBM5 domain gave higher yields compared with their respective solitary catalytic domains. The catalytic domain of *Cj*Chi18C gave higher yields than the catalytic domains of *Cj*Chi18A and *Cj*Chi18B, but all were poor in chitin degradation compared with *Cj*Chi18D.

Analysis of products generated during degradation of α-chitin showed that $CjChi18A_{cat}$ initially produced both GlcNAc and $(GlcNAc)_2$. The product profiles for the other variants ($CjChi18B_{cat}$, $CjChi18B_{cat+CBM5}$, $CjChi18C_{cat}$, $CjChi18D_{cat}$, and $CjChi18D_{cat+CBM5}$) showed mainly $(GlcNAc)_2$ and smaller amounts of GlcNAc (Fig. S3), as is usual for GH18 chitinases. It is noteworthy that the product profile of $CjChi18B_{cat}$ was different from $CjChi18B_{cat+CBM5}$ after 48 h, where GlcNAc is the dominating product for $CjChi18B_{cat}$, whereas $(GlcNAc)_2$ is the dominating product for $CjChi18B_{cat+CBM5}$ (Fig. S3). For $CjChi18A_{cat}$, only GlcNAc was detected after 48 h, indicating an *N*-acetylhexosaminidase activity for this enzyme.

Synergy experiments (Fig. 6) confirmed the dominating role of *Cj*Chi18D in chitin bioconversion and revealed synergistic effects for various enzyme combinations, such as when mixing

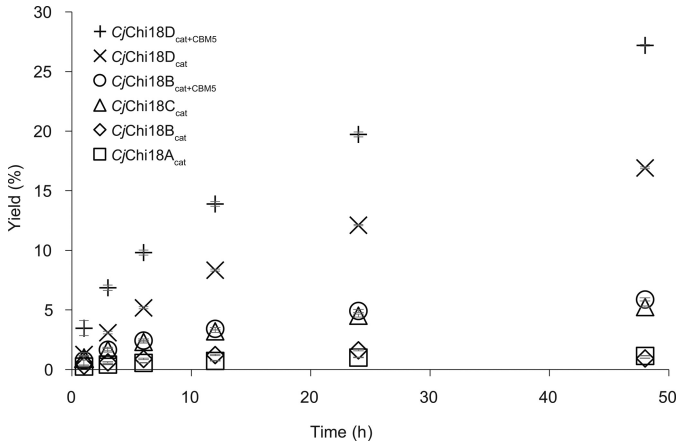

Figure 5. Degradation of α-chitin. Degradation of α-chitin (15 g/liter) at 30 °C was tested in 20 mM BisTris, pH 6.5, 0.1 mg/ml BSA. The enzyme concentration was 0.5 μM, and samples were taken at different time points. The yield refers to the degree of chitin solubilization. The α-chitin used contained 6.43% ash and 5.42% moisture, and this was taken into account when calculating yields. Each reaction was performed in triplicate; standard deviations are shown as *error bars* but are difficult to see because they are low and are partly covered by the *symbols*.

$CjChi18A_{cat}$ with $CjChi18B_{cat}$, $CjChi18B_{cat}$ with $CjChi18C_{cat}$, and $CjChi18B_{cat}$ with $CjChi18D_{cat}$. These synergistic effects indicate that the various chitinases must have different functionalities. As expected on the basis of the data presented above, the presence of $CjChi18A_{cat}$ shifted the product profile toward a higher GlcNAc/$(GlcNAc)_2$ ratio. The effect of adding *Cj*LPMO10A was generally small but seemed slightly larger when combined with the individual catalytic domains of *Cj*Chi18A, *Cj*Chi18B, and *Cj*Chi18C, compared with *Cj*Chi18D. Although *Cj*Chi18D alone was the most potent individual enzyme, the highest chitin solubilization yields were obtained when *Cj*Chi18D was paired with other chitinases.

Investigation of enzyme activity toward soluble chito-oligosaccharides can give insight into preferred substrate binding modes and intrinsic catalytic rates. Thus, activity toward the soluble chito-oligosaccharide $(GlcNAc)_6$ was determined for all four GH18 catalytic domains (Fig. 7*A*). The results indicated that $CjChi18C_{cat}$ had the highest activity against $(GlcNAc)_6$ with an initial rate of $300 \pm 8\ min^{-1}$. $CjChi18A_{cat}$ had an initial rate of $118 \pm 1\ min^{-1}$, whereas $CjChi18D_{cat}$ and $CjChi18B_{cat}$ had initial rates of 44.5 ± 2.6 and $27.0 \pm 0.8\ min^{-1}$, respectively. The product profile obtained for the enzymes shortly after initiation of the $(GlcNAc)_6$ hydrolysis reactions (2-min reaction time) showed striking differences between the chitinases (Fig. 7*B*). $CjChi18A_{cat}$ yielded all possible product types ($(GlcNAc)_{1-5}$), where GlcNAc was the dominating product (97.8 ± 7.3 μM) followed by $(GlcNAc)_2$ (62.3 ± 2.5 μM), $(GlcNAc)_3$ (47.7 ± 1.7 μM) and $(GlcNAc)_4$ (33.9 ± 1.5 μM). Quantification of $(GlcNAc)_5$ was not possible because of co-elution with $(GlcNAc)_6$. $CjChi18B_{cat}$ produced mainly $(GlcNAc)_2$ and $(GlcNAc)_3$, with minor amounts of $(GlcNAc)_4$. $CjChi18C_{cat}$ produced $(GlcNAc)_{2-4}$ and $CjChi18D_{cat}$ produced mainly $(GlcNAc)_2$ and $(GlcNAc)_4$. Chito-oligosaccharides longer than $(GlcNAc)_6$ were observed in the $CjChi18D_{cat}$ reaction (Fig. 7*B* and Fig. S4), indicating that this enzyme has transglycosylating activity. Reactions using $(GlcNAc)_2$ as a substrate showed rapid conversion by $CjChi18A_{cat}$, whereas only trace

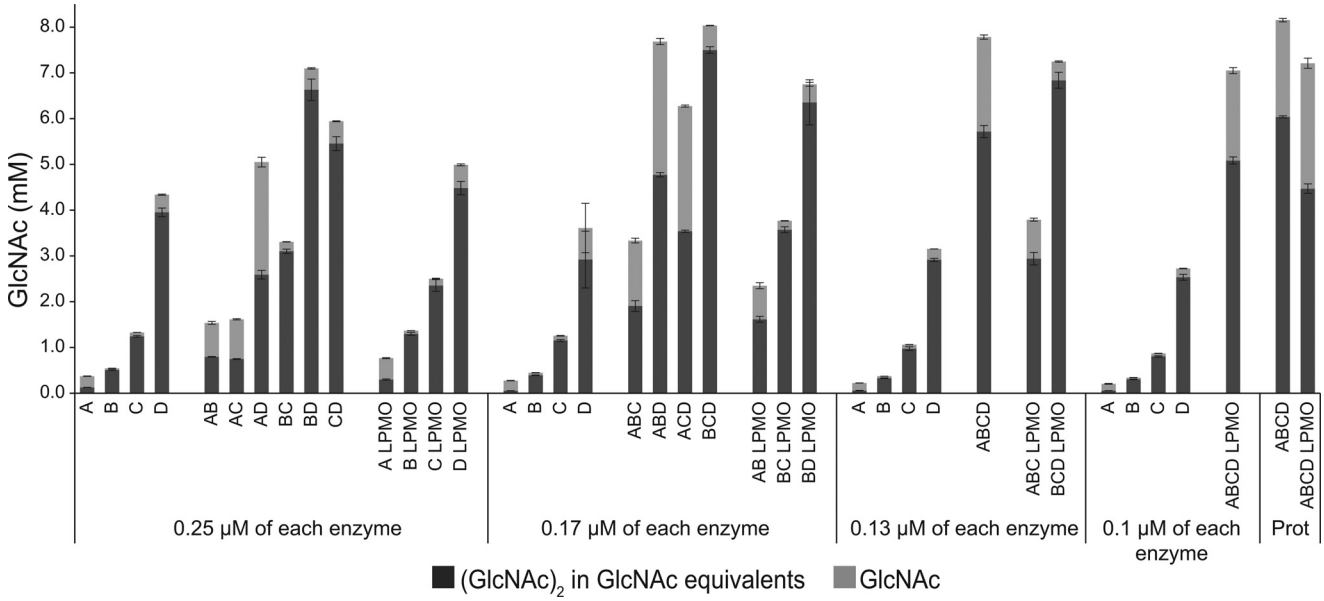

Figure 6. Synergy experiments. The catalytic domains of all chitinases and the *Cj*LPMO10A were mixed in different ways to investigate possible synergistic effects in reactions with α-chitin (15 g/liter). The maximum total enzyme load was 0.5 μM with equal amounts of each enzyme, as indicated in the figure. In the reactions where the ratio was determined by protein quantification data from a previous proteomics study (*Prot*) (22), the total enzyme loading was also 0.5 μM. In the proteomics reaction without *Cj*LPMO10A, the ratio was 21% *Cj*Chi18A, 4% *Cj*Chi18B, 22% *Cj*Chi18C, and 52% *Cj*Chi18D. In the proteomics reaction with *Cj*LPMO10A, the ratio was 14% *Cj*Chi18A, 3% *Cj*Chi18B, 15% *Cj*Chi18C, 35% *Cj*Chi18D, and 33% *Cj*LPMO10A. The *Cj*LPMO10A was Cu^{2+}-saturated before use. Reaction mixtures were incubated at 30 °C in 20 mM BisTris, pH 6.5, 0.1 mg/ml BSA, and samples were taken after 24 h. In reactions with *Cj*LPMO10A, 0.5 mM ascorbate was added as an external electron donor. Production of GlcNAc and $(GlcNAc)_2$ was quantified, and the amount of $(GlcNAc)_2$ is given in GlcNAc equivalents. Three parallel reactions were done for each condition and standard deviations are shown as *error bars*. Reaction mixtures that contained the LPMO showed minor amounts of oxidized $(GlcNAc)_2$, which were not quantified.

amounts of the monomer were detected for the other three chitinase (results not shown).

C. japonicus GH18 chitinase genes are highly expressed during chitin utilization

To obtain further insight into the regulation of chitinase expression and to complement the previous secretome study (22), we used RNAseq to determine changes in gene expression during growth using α-chitin relative to growth using glucose. Analysis of samples from the exponential growth phase revealed significant up-regulation of 73 CAZyme genes (Table S3*A*). The seven most strongly up-regulated genes were all related to chitin bioconversion, including the LPMO (6.7-fold, $\log_2$ scale), the *hex20B* hexosaminidase (4.1-fold), the *nag9A* gene (3.5-fold) that encodes a putative *N*-acetylhexosamine 6-phosphate deacetylase, and the four GH18 chitinases in the following order *chi18D*> *chi18C* > *chi18A* > *chi18B*, the fold change ($\log_2$ scale) being 6.7-, 5.1-, 3.9-, and 3.6-fold, respectively (Fig. 8 and Table S3*A*). Several other genes putatively involved in chitin bioconversion were also up-regulated, albeit to a lesser extent, including the GH19 chitinase (2.2-fold, $\log_2$ scale), the other GH20 hexosaminidase (*hex20A*; 2.7-fold), and the GH46 chitosanase and two polysaccharide deacetylases (2.6-, 1.6-, and 1.4-fold, respectively).

The comparison of gene expression during early stationary phase yielded similar results (Fig. S5*A* and Table S3*B*). This analysis revealed the up-regulation of 47 CAZyme genes, of which seven are implicated in chitin degradation (*lpmo10A*, *chi18D*, *chi18C*, *chi18B*, *nag9A*, *hex20A*, and *chi19A*). Although the expression data, in particular for the exponential comparison, showed a strong up-regulation of chitin-relevant genes, there was also up-regulation of a wide variety of CAZyme genes associated with the degradation of other polysaccharides such as starch, xylan, cellulose, pectin, arabinanan, mannan, β-glucan, and xyloglucan. Therefore, the regulation of the chitin response resembles the general response previously observed for cellulose (14). When comparing the transcriptomes of the exponential and the stationary phase during growth on chitin, none of the significant changes in expression concerned CAZyme genes (Fig. S5*B*).

Discussion

A previous report demonstrated that *C. japonicus* can grow using both purified chitin and unrefined crab shells as a sole nutrient source (13). Additionally, a recent proteomic study found several secreted GH18 chitinases, suggesting a robust response to chitin (22). It has remained unknown, however, how these GH18 chitinases contribute to the degradation of chitin, and to what extent the four GH18 genes in the *C. japonicus* genome are equivalent. In this study, through an implementation of transcriptomic, genetic, and biochemical approaches, we assessed the physiological functions of the four GH18 enzymes. The synthesis of *in vitro*, *in vivo*, and *in silico* data provides a comprehensive understanding of chitin degradation by *C. japonicus*.

The architecture of the family GH18 chitinases indicates differential biological roles

Analysis using LipoP (29) predicts that the *Cj*Chi18A enzyme is a lipoprotein with a signal sequence cleaved by signal peptidase II (SPII). The presence of a glutamine in position +2 after the cleavage site of SPII further suggests that *Cj*Chi18A

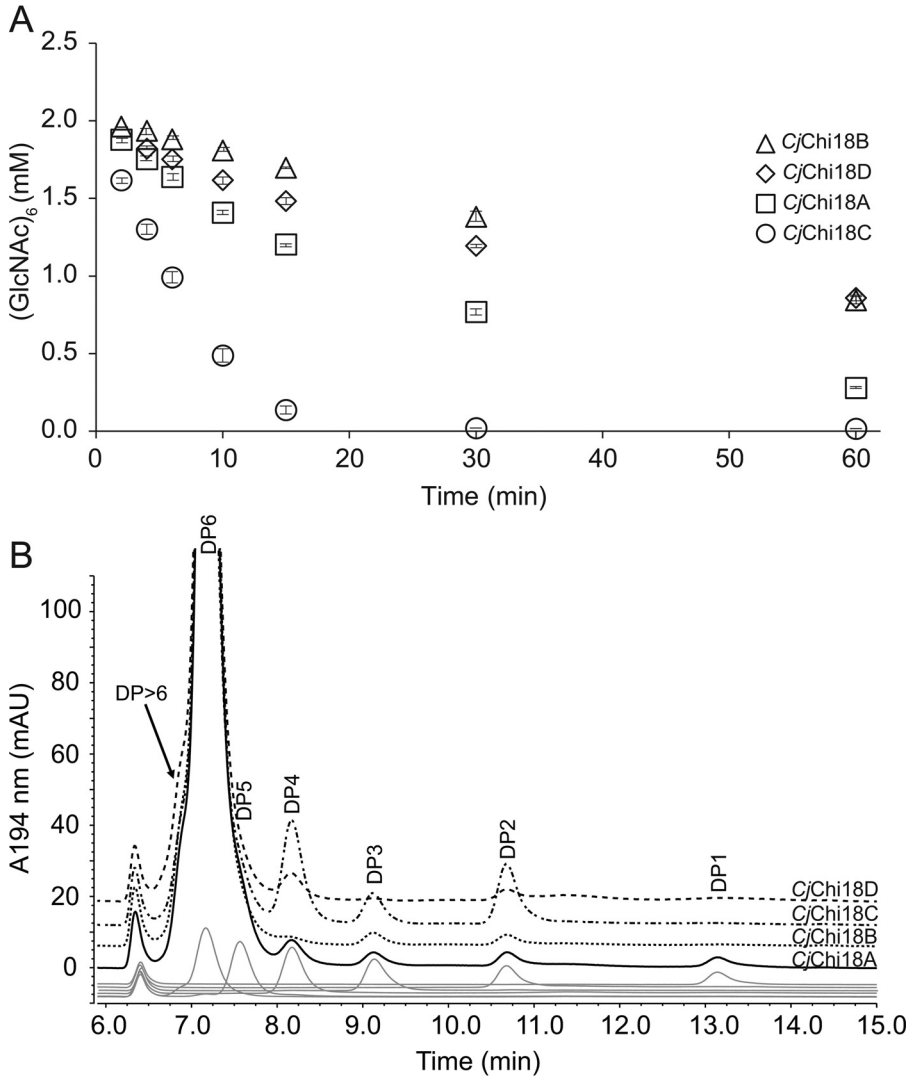

Figure 7. Hydrolysis of $(GlcNAc)_6$. *A*, hydrolysis of $(GlcNAc)_6$ over time. The slopes of the linear parts of these curves were used to calculate the initial rates. Standard deviations are shown as *error bars*. *B*, chromatograms showing the product profile obtained 2 min after mixing chitinases with substrate. *DP1–DP6* represent $(GlcNAc)_{1-6}$. Chromatograms for various standards are shown as *gray lines* at the *bottom*. These experiments were done with the catalytic domains of the chitinases. The reactions contained 2 mM $(GlcNAc)_6$, 10 mM BisTris, pH 6.5, 0.1 mg/ml BSA, and 50 nM enzyme and were done in triplicate at 30 °C. Chromatograms for samples taken after 60 min are shown in Fig. S4.

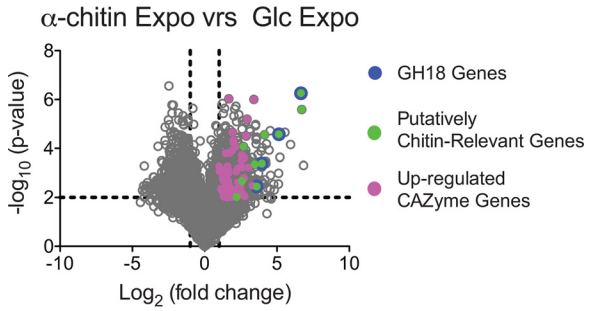

Figure 8. Differential gene expression for *C. japonicus* during exponential growth. This volcano plot shows the $\log_2$(fold change) plotted against the $-\log_{10}$(*p* value) for every gene in *C. japonicus* during exponential growth on glucose compared with α-chitin, where each *gray circle* represents the expression of a single gene. The *black dashed lines* indicate the significance cutoff values: $-\log_{10}(p\text{ value}) > 2$ and $\log_2(\text{fold change}) > 1$. The genes colored *magenta* represent CAZyme genes, and the complete list of these genes can be found in Table S3*A*.

resides attached to the outer membrane (32–35). Interestingly, *Cj*Chi18A was found in high amounts in a recent secretome study (22); however, the precise location of this enzyme remains undefined. It is likely that *Cj*Chi18A functions in degrading short chito-oligosaccharides, because the absence of CBMs limits the association of this enzyme with polymeric chitin (31, 36). Such a function is supported by the biochemical data for *Cj*Chi18A showing high activity on soluble substrates and an ability to produce monomers.

Analysis of the *Cj*Chi18B, *Cj*Chi18C, and *Cj*Chi18D enzymes indicated a signal peptide that is cleaved by signal peptidase I (29). The growth defect on chitin observed in the Δ*gsp* mutant suggests that these three enzymes are transported to the extracellular space by the type II secretion system (37). The *Cj*Chi18B, *Cj*Chi18C, and *Cj*Chi18D enzymes all possess a CBM5 and a CBM73 domain (38); however, the orientations of these domains differ between the enzymes (Fig. 2). As found with many CAZymes, the *Cj*Chi18B, *Cj*Chi18C, and *Cj*Chi18D chitinases contain serine-rich regions separating the individual domains, which likely act as flexible linkers (39).

Analysis of the domain organization of the *C. japonicus* chitinases, functional data, homology modeling of their 3-D structures (Fig. S6), and comparison with well-characterized GH18 chitinases from *Serratia marcescens* (18) all indicate that the *C. japonicus* chitinolytic system represents a suite of complementary activities. Available data from known processive chitinases show that there are hallmarks specific for processive enzymes, involving an $\alpha+\beta$ domain in the structure and conserved aromatic amino acids lining the catalytic cleft (40–43). Structural modeling of the *C. japonicus* GH18 chitinases and sequence alignment with known processive chitinases (Fig. S7) show that *Cj*Chi18B and *Cj*Chi18D have these specifications. *Cj*Chi18B has a large $\alpha+\beta$ domain (~110 amino acids) and a "tunnel-like" substrate-binding cleft, whereas *Cj*Chi18D has a much smaller $\alpha+\beta$ domain (~60 amino acids) and a more open active-site cleft. Compared with the chitinases from *S. marcescens* (Fig. S6), the structural model of *Cj*Chi18B shows a more closed active site than exo-processive *Sm*ChiA and *Sm*ChiB, whereas *Cj*Chi18D seems to have a more open active site cleft than these two *Serratia* enzymes. *Cj*Chi18A has the $\alpha+\beta$ domain (~65 amino acids) but lacks most of the aromatic residues; the most similar *S. marcescens* enzyme seems to be *Sm*ChiD, which, like *Cj*Chi18A, primarily produces monomers (44). *Cj*Chi18C does not have features characteristic for processivity and is more similar to *Sm*ChiC, which is a non-processive endo-chitinase, displaying an open substrate binding cleft that is characteristic for non-processive glycoside hydrolases (36).

The GH18 enzymes of C. japonicus have divergent functionalities but are reliant on CjChi18D

The growth and chitinase secretion data strongly pointed to the *chi18D* gene product being essential for the degradation of chitinous substrates (Figs. 3 and 4 and Fig. S2). These results reinforce two features previously described for *C. japonicus*, specifically, that secreted enzymes are essential for recalcitrant polysaccharide degradation and that single CAZymes elicit major physiological effects (27, 45–47). Other individual enzymes did not seem essential for growth, but the Δ*chi18B* Δ*chi18C* double deletion mutant did show reduced growth and reduced chitin conversion efficiency (Figs. 3 and 4), indicating that these two chitinases have complementing functionalities and that they contribute to chitin conversion but are not essential. The absence of growth defects of the multiple mutants while growing using crab shells is likely a consequence of the slow overall growth rate.

Biochemical characterization of the catalytic domains revealed clear functional differences (Figs. 5 and 7, Fig. S4, and Table S4) and showed that the GH18 enzymes act synergistically during the degradation of chitin (Fig. 6). Enzyme synergy during the course of chitin degradation has been described previously for *S. marcescens* and is generally ascribed to collaboration between endo- and exo-acting enzymes, where endo-acting enzymes generate chain ends that are substrates for exo-acting enzymes that usually show processive action (48). The synergistic effects observed for the best combinations of *C. japonicus* chitinases (Fig. 6) are of similar size as the effects observed for the *S. marcescens* enzymes (49, 50). It is worth noting that the clearest synergy was observed when combining *Cj*Chi18B, for which there are strong indications of exo-processive action, and *Cj*Chi18C or *Cj*Chi18D, which both could be endo-acting enzymes (*vide infra*). Previous studies with β-chitin have shown that culture supernatants of chitin-grown *S. marcescens* and chitin-grown *C. japonicus* have similar chitinolytic power (22).

The GH18 chitinases exhibit processivity during chitin hydrolysis

Although it is difficult to determine the degree of processivity from standard substrate degradation experiments, such experiments do provide indications. During degradation of crystalline chitin, processive enzymes tend to generate high $(GlcNAc)_2$/GlcNAc ratios (43, 51). Furthermore, the degradation of $(GlcNAc)_6$ by processive enzymes will yield a high $(GlcNAc)_2/(GlcNAc)_4$ ratio because such enzymes will process the chitohexaose into three chitobiose moieties rather than releasing the chitotetraose and chitobiose into solution after a single hydrolytic event (as would be expected for a non-processive enzyme). Of the GH18 chitinases of *C. japonicus*, only *Cj*Chi18B showed these high ratios (Table S4), indicating that this enzyme is the most processive, as also suggested by the structural model discussed above (Fig. S6). The other three enzymes did not show clear signs of processivity. *Cj*Chi18C displays all hallmarks of a non-processive enzyme, and *Cj*Chi18A is unique because it primarily produces monomers, which is not really compatible with processivity because the repeating unit in a chitin chain is a dimer. These latter two enzymes showed the highest specific activities toward the hexamer, suggesting that they primarily act on soluble substrates. On the basis of the experimental data, it is difficult to judge whether the four enzymes are endo- or exo-acting, and it should be noted that mixed endo-/exo-modes do occur (52). *Cj*Chi18B appears to be exo-processive, whereas *Cj*Chi18C looks to be endo-non-processive. The situation for *Cj*Chi18A and *Cj*Chi18D is less clear, because the deep but still relatively open active site clefts of these enzymes are compatible with both endo- and exo-action and because the biochemical data were not conclusive regarding processivity.

The chitinolytic machinery of C. japonicus is highly responsive to the presence of chitin substrates

There was significant up-regulation of the predicted *C. japonicus* genes encoding chitin-active proteins (GH18, GH19, GH20, GH46, and AA10 families) during both the exponential phase and the stationary phase (Table S3). The up-regulation of a number of other CAZyme genes not involved in chitin degradation was striking but not surprising. *C. japonicus* has been shown to have both substrate-dependent and growth rate-dependent control of CAZyme gene expression (14). In regards to the substrate-specific response, *C. japonicus* seems to have two variations: one that is general (where diverse CAZyme genes are up-regulated) and one that is specific (where only substrate-specific CAZymes genes are up-regulated). The response observed for cellulose is an example of the former (14), and the response for xylan is the latter (46). The regulatory network for the chitinolytic response appears to be

analogous to the cellulose response, which is not surprising given the similarities of the substrates.

The expression data also indicated that the most up-regulated chitin-relevant gene encodes the chitin-specific LPMO, *Cj*LPMO10A. It has been shown that this enzyme will act synergistically with chitinases (13) but in the present study, the effects of adding the LPMO to the chitinases was limited (Fig. 6). This is likely an effect of the substrate used in this study, which was ball-milled into fine particles. It has previously been shown that such ball-milling reduces the crystallinity of the substrate, hence reducing the activity of the LPMO (53).

Final remarks

The proposed model (Fig. 1) for crystalline chitin degradation by *C. japonicus,* based on *in vitro*, *in vivo*, and *in silico* analyses is that the four GH18 chitinases and *Cj*LPMO10A synergistically degrade chitin. *Cj*LPMO10A plays an important role, as indicated by the transcriptomic data presented here and previously published biochemical data (13). *Cj*Chi18D, being the most powerful chitin degrader, likely also acts on the more recalcitrant parts of the substrate, releasing chito-oligosaccharides. *Cj*Chi18B and *Cj*Chi18C act on the more accessible chitin fibers, converting them into smaller chito-oligosaccharides, whereas *Cj*Chi18A converts chito-oligosaccharides to *N*-acetylglucosamine.

Experimental procedures

Growing conditions

C. japonicus strains were grown using MOPS minimal medium (54) containing 0.2% w/v glucose, 0.5% w/v *N*-acetylglucosamine, 0.25% (w/v) α-chitin from shrimp shells (Sigma–Aldrich), 0.2% (w/v) β-chitin from squid pen, or 4% (w/v) crab shells from *Callinectes sapidus* as the sole source of carbon. The following protocols were developed to prepare the chitin containing substrates. The coarse flakes of α-chitin were sieved through the top piece of a 130-mm Buchner polypropylene filter to homogenize the particle size (diameter of ~4 mm). β-Chitin from squid pen was manually ground in a ceramic mortar and pestle and then passed through a plastic filter with 4-mm diameter holes. For the crab shells, any membranous material was discarded, and the shells were then thoroughly washed and rinsed. Clean and air-dried shells were manually ground and then sieved through a 4-mm diameter filter. To remove any generated crab shell dust, the filtrate was rinsed through a Buchner polypropylene filter. The shell pieces were subjected to autoclave sterilization. *Escherichia coli* strains were grown using lysogenic broth (55). For growth analysis studies, the strains were initially grown for 24 h in 5 ml of MOPS–glucose medium. Then an 18-mm test tube with 5 ml of MOPS–chitin broth was inoculated with a 1:100 dilution of the prepared overnight cultures. All cultures were incubated at 30 °C with an aeration of 225 RPM. For insoluble substrates, growth was measured as a function of the A_{600} value with a Spec20D+ spectrophotometer (Thermo Scientific) using biomass containment as needed (56). In growth experiments with glucose or *N*-acetylglucosamine, growth was monitored using a Tecan M200Pro microplate reader at 600 nm (A_{600}) (Tecan Trading AG, Switzerland). All growth experiments were performed in biological triplicate. Plate media were solidified with 1.5% agar. When required, kanamycin was used at a concentration of 50 μg/ml.

Generation of deletion mutants

Deletion mutants of the family GH18 chitinases of *C. japonicus* were made and verified using previously published protocols (27, 45). A suicide vector was generated by cloning ±500 bp up- and downstream from the gene to be deleted into the pK18*mobsacB* vector (57) at the EcoRI and the XbaI sites. The pK18*mobsacB* plasmids to make the deletions of genes *chi18A*, *chi18B*, and *chi18C* were synthetized by GeneWiz (South Plainfield, NJ), whereas the plasmid to make the deletion of *chi18D* was amplified by PCR and constructed via Gibson assembly (58). All vectors were electroporated into *E. coli* S17 λ_{PIR}. Through tri-parental mating, the deletion plasmid was conjugated into *C. japonicus* using an *E. coli* helper strain containing the plasmid pRK2013 (59). Recombinant colonies were selected using kanamycin selection, with a counter selection carried out via sucrose toxicity. The deletion mutants were confirmed by PCR, and the primers used for the construction and verification of *C. japonicus* mutants are listed in Table S5.

Visualization of colloidal chitin degradation

Colloidal chitin was prepared as described in (60). Colloidal chitin plates were made using MOPS-defined medium supplemented with 2% (w/v) colloidal chitin and 0.2% (w/v) glucose. To assay for chitin degradation, 10 μl of overnight cultures of the *C. japonicus* strains to be analyzed were spotted onto the chitin plate and incubated for 4 days at 30 °C. Then the plates were stained with a 0.1% (w/v) Congo red solution for 10 min followed by 10 min destaining with a 1 M NaCl solution, as described previously for detection of degradation of carboxyl methyl cellulose (27, 45, 56).

Transcriptomic analysis

A transcriptomic analysis was conducted for *C. japonicus* grown using glucose or α-chitin. To prepare the samples, the protocol described by Gardner *et al.* (14) was followed. Briefly, 35 ml of cell culture were aliquoted into 50-ml conical tubes with 5 ml of a stopping solution made with ethanol and saturated phenol (19:1). The cells were pelleted by centrifugation at 8000 × *g* for 5 min at 4 °C. The supernatant was removed, and the cell pellets were immersed in a dry ice/ethanol bath for 5 min. The frozen cell pellets were then stored at −80 °C. For each carbon source, the samples were taken in biological triplicate and at two time points: the beginning of the exponential phase ($0.1 > A_{600} > 0.2$) and the beginning stationary phase. GeneWiz performed RNAseq using an Illumina HiSeq2500 (50-bp single-reads; >10 million reads/sample), and sequence data were analyzed using CLC Genomics Workbench (Qiagen). The $\log_2$ transformation and a Student's *t* test were used for the comparative analysis of *C. japonicus* gene expression. An adjusted *p* value > 0.01 and a $\log_2$ fold change > 2 were selected as significance cutoff parameters. RNAseq data for glucose grown *C. japonicus* cells (GSE90955) was used as done previously (26). The chitin-specific RNAseq data that was generated

for this study can be found in the NCBI GEO database (GSE108935).

Bioinformatics analysis

We determined the predicted CAZy domains presented using the Database for Automated Carbohydrate-Active Enzyme Annotation (38). Using LipoP (29) and SignalP (30), we determined the putative location of the chitinolytic enzymes. Three-dimensional models of the GH18 chitinases were generated using PyMod 2.0 (61).

Cloning and expression of chitinases

Synthetic genes of the four full-length chitinases, optimized for expression in *E. coli*, were purchased from GeneScript. These genes encoded the catalytic domain for *Cj*Chi18A and the full-length protein (without signal peptide) for *Cj*Chi18B, *Cj*Chi18C, and *Cj*Chi18D. Primers for amplification of the genes were designed so that a His_6 tag followed by a TEV protease cleavage site was introduced at the N terminus of all proteins and a stop codon was introduced before the C-terminal His tag encoded in the vector. Using different primers for amplification, genes encoding different versions (Table S6) of the modular proteins were generated, which were cloned into the pNIC-CH vector (62) using ligation independent cloning (63). The DNA sequences of the genes were confirmed by Sanger sequencing. Plasmids were transformed into *E. coli* BL21 cells. Protein expression was tested by inoculating 50 ml of lysogenic broth + 50 μg/ml kanamycin with 500 μl of an overnight culture. The cultures were grown at 37 °C, and when the OD reached 0.6, the cells were induced by adding IPTG to a final concentration of 0.2 mM. After growth overnight at 30 °C, the cells was harvested by centrifugation (6164 × *g*, 12 min, 4 °C) and resuspended in 5 ml of 20 mM Tris-HCl, 150 mM NaCl, 5 mM imidazole, pH 8.0. DNaseI and PMSF were added to final concentrations of 1.4 μg/ml and 0.1 mM, respectively, before the cells were lysed by sonication (pulse 3 s on, 3 s off for 3–5 min), using a VC750 VibraCell sonicator (Sonics & Materials, Inc.). Following cell disruption, the samples were centrifuged (11,814 × *g*, 12 min, 4 °C), after which the supernatant was collected and filtrated (0.22 μm). Analysis by SDS-PAGE showed that only *Cj*Chi18A was soluble. Except for the full-length enzymes, which were not produced in detectable levels, all other enzyme variants were produced in large amounts but were insoluble.

Production of *Cj*Chi18A was scaled up to a 500-ml culture following the same protocol as above for production and harvesting. The filtrated supernatant containing *Cj*Chi18A was used for protein purification by nickel affinity chromatography using a HisTrap HP 5 ml column (GE Healthcare Life Sciences) connected to an Äkta pure system (GE Healthcare Life Sciences). A continuous imidazole gradient ending at 300 mM imidazole was used to elute bound protein, using a flow rate of 1 ml/min.

*Cj*Chi18B_{cat}, *Cj*Chi18$B_{cat+CBM5}$, *Cj*Chi18C_{cat}, *Cj*Chi18D_{cat}, and *Cj*Chi18$D_{cat+CBM5}$ were produced using a denaturing and refolding method, starting with 500-ml cultures as described above. After harvesting the cells (7025 × *g*, 12 min, 4 °C), the pellet was resuspended in 20 ml of 50 mM Tris, pH 8.0, 0.2 M NaCl, and 50% of the cell suspension was used in the further steps. After another centrifugation (18,459 × *g*, 10 min, 4 °C), the pellet was resuspended in 10 ml of 50 mM Tris, pH 8.0, 0.2 M NaCl and, after addition of lysozyme (final concentration, 200 μg/ml) and DNaseI (final concentration 0.1 mM), the samples were incubated on ice for 30 min. The samples were subsequently sonicated (pulse 3 s on, 3 s off, 2–4 min), and inclusion bodies were harvested by centrifugation (18,459 × *g*, 10 min), after which the protein pellet was resuspended in 25 ml of washing buffer (20 mM Tris-HCl, 100 mM NaCl, 2% Triton X-100, pH 8.0). The centrifugation and subsequent resuspension in washing buffer steps were repeated twice, and after the final centrifugation, the pellet was dissolved in 5 ml of cold denaturing solution (50 mM Tris-HCl, pH 8.5, 100 mM NaCl, 5 M guanidine HCl, 1 mM EDTA, and 20 mM DTT), vortexed for 1 min, and incubated overnight at 4 °C with slow rotation of the sample tubes. The samples were then centrifuged at 9000 × *g* for 10 min at 4 °C. The supernatant containing the denatured protein was then collected for refolding.

The sample containing the denatured protein (~5 ml) was added to 250 ml of cold refolding buffer (100 mM Tris-HCl, 0.4 M L-arginine, 0.5 mM oxidized glutathione, 5 mM reduced glutathione) at a rate of 1 ml/h under intense stirring at 4 °C. After adding all protein, the solution was stirred overnight at 4 °C, before centrifugation (9000 × *g*, 10 min, 4 °C). The supernatant was collected and dialyzed (10-kDa molecular mass cutoff Snakeskin; Thermo Fisher Scientific) against 2.5 liters of 50 mM Tris-HCl, 0.1 M NaCl, pH 8.0, overnight. The dialysis solution was changed once, after ~6 h. After collecting the dialyzed sample, the protein was purified with nickel affinity chromatography as described above. All refolded proteins stayed soluble during these procedures, and the yields of recovered purified soluble protein were typically 1–5 mg/liter culture.

The presence and purity of the proteins was confirmed by SDS-PAGE, and relevant fractions were pooled before the protein solution was concentrated to 26.4 mg/ml for *Cj*Chi18A and 1–3.5 mg/ml for the unfolded/refolded chitinases, with concomitant buffer exchange to 50 mM Tris-HCl, 100 mM NaCl, pH 8.0, using Amicon Ultra-15 centrifugal filters with 10,000 Nominal Molecular Weight Limit (Merck Millipore). All resulting protein solutions were stable for weeks at 4 °C. Protein concentrations were determined by measuring the absorbance at 280 nm and using the theoretical extinction coefficient (calculated using the ExPASy ProtParam tool available from https://web.expasy.org/protparam). The catalytic domain of *Cj*LPMO10A was expressed and purified as previously described by Forsberg *et al.* (13).

Activity assays

Standard reactions contained 15 g/liter α-chitin (extracted from *Pandalus borealis*; Seagarden, Karmsund, Norway) or 2 mM chito-oligosaccharides (MegaZyme, Bray, Ireland), 0.1 mg/ml BSA and 20 mM BisTris, pH 6.5, unless stated otherwise. For chitin degradation 0.5 μM enzyme was used, whereas for chito-oligosaccharide degradation 50 nM enzyme was used, unless stated otherwise. The reaction mixtures were incubated in a thermomixer at 30 °C and 800 rpm, and enzyme activity was quenched by adding sulfuric acid to a final concentration of

25 mM. A Rezex RFQ fast acid H+ (8%) ion-exclusion column (Phenomenex) installed on a Dionex Ultimate 3000 HPLC with UV detection (194 nm) was used to analyze and quantify degradation products as described by Mekasha *et al.* (64). Conversion yields were calculated as percentages of the theoretical maximum after correction of the amount of chitin in the reaction for ash and water content. Reactions with $(GlcNAc)_6$ as substrate were analyzed using a Rezex ROA-organic acid H+ (8%) ion exclusion column (Phenomenex) installed on a Dionex Ultimate 3000 HPLC, using a column temperature of 65 °C. An 8-μl sample was injected on the column, and the mono/oligosaccharides were eluted isocratically at 0.6 ml/min with 5 mM sulfuric acid as mobile phase. The chito-oligosaccharides were monitored by measuring the absorbance at 194 nm. Standards with known concentrations of GlcNAc (Sigma) and $(GlcNAc)_{2-6}$ (MegaZyme) were used to determine the concentrations of $(GlcNAc)_6$ and the degradation products.

Author contributions—E. C. M. and T. R. T. formal analysis; E. C. M. and T. R. T. investigation; E. C. M. and T. R. T. visualization; E. C. M. and T. R. T. methodology; E. C. M., T. R. T., G. V.-K., V. G. H. E., and J. G. G. writing-original draft; E. C. M., T. R. T., G. V.-K., V. G. H. E., and J. G. G. writing-review and editing; G. V.-K., V. G. H. E., and J. G. G. supervision; G. V.-K., V. G. H. E., and J. G. G. project administration; J. G. G. conceptualization; G. V.-K., V. G. H. E., and J. G. G. funding acquisition.

Acknowledgments—We thank C. E. Nelson for assistance with the collection of the RNAseq samples and A. D. Blake for technical support.

References

1. Gooday, G. W., Humphreys, A. M., and McIntosh, W. H. (1986) Roles of chitinases in fungal growth. In *Chitin in Nature and Technology* (Muzzarelli, R., Jeuniaux, C., and Gooday, G. W., eds.) pp. 83–91, Springer-Verlag, New York Inc., New York
2. Beier, S., and Bertilsson, S. (2013) Bacterial chitin degradation-mechanisms and ecophysiological strategies. *Front. Microbiol.* **4,** 149 Medline
3. Khor, E., and Lim, L. Y. (2003) Implantable applications of chitin and chitosan. *Biomaterials* **24,** 2339–2349 CrossRef Medline
4. Francesko, A., and Tzanov, T. (2011) Chitin, chitosan and derivatives for wound healing and tissue engineering. *Adv. Biochem. Eng. Biotechnol.* **125,** 1–27 Medline
5. Matroodi, S., Motallebi, M., Zamani, M., and Moradyar, M. (2013) Designing a new chitinase with more chitin binding and antifungal activity. *World J. Microbiol. Biotechnol.* **29,** 1517–1523 CrossRef Medline
6. Stoykov, Y. M., Pavlov, A. I., and Krastanov, A. I. (2015) Chitinase biotechnology: production, purification, and application. *Eng. Life Sci.* **15,** 30–38 CrossRef
7. Yan, N. (2017) Sustainability: don't waste seafood waste. *Nature* **524,** 155–157 Medline
8. Yan, Q., and Fong, S. S. (2015) Bacterial chitinase: nature and perspectives for sustainable bioproduction. *Bioresources Bioprocessing* **2,** 31 CrossRef
9. Tharanathan, R. N., and Kittur, F. S. (2003) Chitin: the undisputed biomolecule of great potential. *Crit. Rev. Food Sci. Nutr.* **43,** 61–87 CrossRef Medline
10. Gortari, M. C., and Hours, R. A. (2013) Biotechnological processes for chitin recovery out of crustacean waste: a mini-review. *Electron J. Biotechnol.* **16,** 10.2225/vol16-issue3-fulltext-10 CrossRef
11. Hemsworth, G. R., Déjean, G., Davies, G. J., and Brumer, H. (2016) Learning from microbial strategies for polysaccharide degradation. *Biochem. Soc. Trans.* **44,** 94–108 CrossRef Medline
12. Zargar, V., Asghari, M., and Dashti, A. (2015) A review on chitin and chitosan polymers: structure, chemistry, solubility, derivatives, and applications. *ChemBioEng Rev.* **2,** 204–226 CrossRef
13. Forsberg, Z., Nelson, C. E., Dalhus, B., Mekasha, S., Loose, J. S., Crouch, L. I., Røhr, A. K., Gardner, J. G., Eijsink, V. G., and Vaaje-Kolstad, G. (2016) Structural and functional analysis of a lytic polysaccharide monooxygenase important for efficient utilization of chitin in *Cellvibrio japonicus*. *J. Biol. Chem.* **291,** 7300–7312 CrossRef Medline
14. Gardner, J. G., Crouch, L., Labourel, A., Forsberg, Z., Bukhman, Y. V., Vaaje-Kolstad, G., Gilbert, H. J., and Keating, D. H. (2014) Systems biology defines the biological significance of redox-active proteins during cellulose degradation in an aerobic bacterium. *Mol. Microbiol.* **95,** 418–433 Medline
15. Vaaje-Kolstad, G., Westereng, B., Horn, S. J., Liu, Z., Zhai, H., Sørlie, M., and Eijsink, V. G. (2010) An oxidative enzyme boosting the enzymatic conversion of recalcitrant polysaccharides. *Science* **330,** 219–222 CrossRef Medline
16. Meibom, K. L., Li, X. B., Nielsen, A. T., Wu, C. Y., Roseman, S., and Schoolnik, G. K. (2004) The *Vibrio cholerae* chitin utilization program. *Proc. Natl. Acad. Sci. U.S.A.* **101,** 2524–2529 CrossRef Medline
17. Vaaje-Kolstad, G., Bøhle, L. A., Gåseidnes, S., Dalhus, B., Bjorås, M., Mathiesen, G., and Eijsink, V. G. (2012) Characterization of the chitinolytic machinery of *Enterococcus faecalis* V583 and high-resolution structure of its oxidative CBM33 enzyme. *J. Mol. Biol.* **416,** 239–254 CrossRef Medline
18. Vaaje-Kolstad, G., Horn, S. J., Sørlie, M., and Eijsink, V. G. (2013) The chitinolytic machinery of *Serratia marcescens*: a model system for enzymatic degradation of recalcitrant polysaccharides. *FEBS J.* **280,** 3028–3049 CrossRef Medline
19. Gardner, J. G., and Keating, D. H. (2012) Genetic and functional genomic approaches for the study of plant cell wall degradation in *Cellvibrio japonicus*. *Methods Enzymol.* **510,** 331–347 CrossRef Medline
20. Gardner, J. G. (2016) Polysaccharide degradation systems of the saprophytic bacterium *Cellvibrio japonicus*. *World J. Microbiol. Biotechnol.* **32,** 121–132 CrossRef Medline
21. DeBoy, R. T., Mongodin, E. F., Fouts, D. E., Tailford, L. E., Khouri, H., Emerson, J. B., Mohamoud, Y., Watkins, K., Henrissat, B., Gilbert, H. J., and Nelson, K. E. (2008) Insights into plant cell wall degradation from the genome sequence of the soil bacterium *Cellvibrio japonicus*. *J. Bacteriol.* **190,** 5455–5463 CrossRef Medline
22. Tuveng, T. R., Arntzen, M. Ø., Bengtsson, O., Gardner, J. G., Vaaje-Kolstad, G., and Eijsink, V. G. (2016) Proteomic investigation of the secretome of *Cellvibrio japonicus* during growth on chitin. *Proteomics* **16,** 1904–1914 CrossRef Medline
23. Itoh, Y., Kawase, T., Nikaidou, N., Fukada, H., Mitsutomi, M., Watanabe, T., and Itoh, Y. (2002) Functional analysis of the chitin-binding domain of a family 19 chitinase from *Streptomyces griseus* HUT6037: substrate-binding affinity and cis-dominant increase of antifungal function. *Biosci. Biotechnol. Biochem.* **66,** 1084–1092 CrossRef Medline
24. Hoell, I. A., Dalhus, B., Heggset, E. B., Aspmo, S. I., and Eijsink, V. G. (2006) Crystal structure and enzymatic properties of a bacterial family 19 chitinase reveal differences from plant enzymes. *FEBS J.* **273,** 4889–4900 CrossRef Medline
25. Cantarel, B. L., Coutinho, P. M., Rancurel, C., Bernard, T., Lombard, V., and Henrissat, B. (2009) The Carbohydrate-Active EnZymes database (CAZy): an expert resource for Glycogenomics. *Nucleic Acids Res.* **37,** D233–D238 CrossRef Medline
26. Nelson, C. E., Rogowski, A., Morland, C., Wilhide, J. A., Gilbert, H. J., and Gardner, J. G. (2017) Systems analysis in *Cellvibrio japonicus* resolves predicted redundancy of β-glucosidases and determines essential physiological functions. *Mol. Microbiol.* **104,** 294–305 CrossRef Medline
27. Nelson, C. E., and Gardner, J. G. (2015) In-frame deletions allow functional characterization of complex cellulose degradation phenotypes in *Cellvibrio japonicus*. *Appl. Environ. Microbiol.* **81,** 5968–5975 CrossRef Medline
28. Altschul, S. F., Gish, W., Miller, W., Myers, E. W., and Lipman, D. J. (1990) Basic local alignment search tool. *J. Mol. Biol.* **215,** 403–410 CrossRef Medline

29. Juncker, A. S., Willenbrock, H., Von Heijne, G., Brunak, S., Nielsen, H., and Krogh, A. (2003) Prediction of lipoprotein signal peptides in Gram-negative bacteria. *Protein Sci.* **12,** 1652–1662 CrossRef Medline
30. Petersen, T. N., Brunak, S., von Heijne, G., and Nielsen, H. (2011) SignalP 4.0: discriminating signal peptides from transmembrane regions. *Nature Methods* **8,** 785–786 CrossRef Medline
31. Boraston, A. B., Bolam, D. N., Gilbert, H. J., and Davies, G. J. (2004) Carbohydrate-binding modules: fine-tuning polysaccharide recognition. *Biochem. J.* **382,** 769–781 CrossRef Medline
32. Wang, G., Chen, H., Xia, Y., Cui, J., Gu, Z., Song, Y., Chen, Y. Q., Zhang, H., and Chen, W. (2013) How are the non-classically secreted bacterial proteins released into the extracellular milieu? *Curr. Microbiol.* **67,** 688–695 CrossRef Medline
33. Bendtsen, J. D., Kiemer, L., Fausbøll, A., and Brunak, S. (2005) Non-classical protein secretion in bacteria. *BMC Microbiol.* **5,** 58 CrossRef Medline
34. Bendtsen, J. D., Jensen, L. J., Blom, N., Von Heijne, G., and Brunak, S. (2004) Feature-based prediction of non-classical and leaderless protein secretion. *Protein Eng. Des. Sel.* **17,** 349–356 CrossRef Medline
35. Seydel, A., Gounon, P., and Pugsley, A. P. (1999) Testing the "+2 rule" for lipoprotein sorting in the *Escherichia coli* cell envelope with a new genetic selection. *Mol. Microbiol.* **34,** 810–821 CrossRef Medline
36. Payne, C. M., Baban, J., Horn, S. J., Backe, P. H., Arvai, A. S., Dalhus, B., Bjørås, M., Eijsink, V. G., Sørlie, M., Beckham, G. T., and Vaaje-Kolstad, G. (2012) Hallmarks of processivity in glycoside hydrolases from crystallographic and computational studies of the *Serratia marcescens* chitinases. *J. Biol. Chem.* **287,** 36322–36330 CrossRef Medline
37. Nakai, K., and Kanehisa, M. (1991) Expert system for predicting protein localization sites in Gram-negative bacteria. *Proteins* **11,** 95–110 CrossRef Medline
38. Yin, Y., Mao, X., Yang, J., Chen, X., Mao, F., and Xu, Y. (2012) dbCAN: a web resource for automated carbohydrate-active enzyme annotation. *Nucleic Acids Res.* **40,** W445–W451 CrossRef Medline
39. Black, G. W., Rixon, J. E., Clarke, J. H., Hazlewood, G. P., Theodorou, M. K., Morris, P., and Gilbert, H. J. (1996) Evidence that linker sequences and cellulose-binding domains enhance the activity of hemicellulases against complex substrates. *Biochem. J.* **319,** 515–520 CrossRef Medline
40. Perrakis, A., Tews, I., Dauter, Z., Oppenheim, A. B., Chet, I., Wilson, K. S., and Vorgias, C. E. (1994) Crystal structure of a bacterial chitinase at 2.3 A resolution. *Structure* **2,** 1169–1180 CrossRef Medline
41. van Aalten, D. M., Synstad, B., Brurberg, M. B., Hough, E., Riise, B. W., Eijsink, V. G., and Wierenga, R. K. (2000) Structure of a two-domain chitotriosidase from *Serratia marcescens* at 1.9-Å resolution. *Proc. Natl. Acad. Sci. U.S.A.* **97,** 5842–5847 CrossRef Medline
42. Horn, S. J., Sikorski, P., Cederkvist, J. B., Vaaje-Kolstad, G., Sørlie, M., Synstad, B., Vriend, G., Vårum, K. M., and Eijsink, V. G. (2006) Costs and benefits of processivity in enzymatic degradation of recalcitrant polysaccharides. *Proc. Natl. Acad. Sci. U.S.A.* **103,** 18089–18094 CrossRef Medline
43. Zakariassen, H., Aam, B. B., Horn, S. J., Vårum, K. M., Sørlie, M., and Eijsink, V. G. (2009) Aromatic residues in the catalytic center of chitinase A from *Serratia marcescens* affect processivity, enzyme activity, and biomass converting efficiency. *J. Biol. Chem.* **284,** 10610–10617 CrossRef Medline
44. Tuveng, T. R., Hagen, L. H., Mekasha, S., Frank, J., Arntzen, M. Ø., Vaaje-Kolstad, G., and Eijsink, V. G. H. (2017) Genomic, proteomic and biochemical analysis of the chitinolytic machinery of *Serratia marcescens* BJL200. *Biochim. Biophys. Acta* **1865,** 414–421 CrossRef Medline
45. Gardner, J. G., and Keating, D. H. (2010) Requirement of the type II secretion system for utilization of cellulosic substrates by *Cellvibrio japonicus*. *Appl. Environ. Microbiol.* **76,** 5079–5087 CrossRef Medline
46. Blake, A. D., Beri, N. R., Guttman, H. S., Cheng, R., and Gardner, J. G. (2017) The complex physiology of *Cellvibrio japonicus* xylan degradation relies on a single cytoplasmic beta-xylosidase for xylo-oligosaccharide utilization. *Mol. Microbiol.* 10.1111/mmi.13903 CrossRef
47. Nelson, C. E., Attia, M. A., Rogowski, A., Morland, C., Brumer, H., and Gardner, J. G. (2017) Comprehensive functional characterization of the glycoside hydrolase family 3 enzymes from *Cellvibrio japonicus* reveals unique metabolic roles in biomass saccharification. *Environ. Microbiol.* **19,** 5025–5039 CrossRef Medline
48. Jalak, J., Kurasin, M., Teugjas, H., and Väljamäe, P. (2012) Endo-exo synergism in cellulose hydrolysis revisited. *J. Biol. Chem.* **287,** 28802–28815 CrossRef Medline
49. Suzuki, K., Sugawara, N., Suzuki, M., Uchiyama, T., Katouno, F., Nikaidou, N., and Watanabe, T. (2002) Chitinases A, B, and C1 of *Serratia marcescens* 2170 produced by recombinant *Escherichia coli*: enzymatic properties and synergism on chitin degradation. *Biosci. Biotechnol. Biochem.* **66,** 1075–1083 CrossRef Medline
50. Vaaje-Kolstad, G., Horn, S. J., van Aalten, D. M., Synstad, B., and Eijsink, V. G. (2005) The non-catalytic chitin-binding protein CBP21 from *Serratia marcescens* is essential for chitin degradation. *J. Biol. Chem.* **280,** 28492–28497 CrossRef Medline
51. Horn, S. J., Sørbotten, A., Synstad, B., Sikorski, P., Sørlie, M., Vårum, K. M., and Eijsink, V. G. (2006) Endo/exo mechanism and processivity of family 18 chitinases produced by *Serratia marcescens*. *FEBS J.* **273,** 491–503 CrossRef Medline
52. Sikorski, P., Sørbotten, A., Horn, S. J., Eijsink, V. G., and Vårum, K. M. (2006) *Serratia marcescens* chitinases with tunnel-shaped substrate-binding grooves show endo activity and different degrees of processivity during enzymatic hydrolysis of chitosan. *Biochemistry* **45,** 9566–9574 CrossRef Medline
53. Nakagawa, Y. S., Eijsink, V. G., Totani, K., and Vaaje-Kolstad, G. (2013) Conversion of α-chitin substrates with varying particle size and crystallinity reveals substrate preferences of the chitinases and lytic polysaccharide monooxygenase of *Serratia marcescens*. *J. Agric. Food Chem.* **61,** 11061–11066 CrossRef Medline
54. Neidhardt, F. C., Bloch, P. L., and Smith, D. F. (1974) Culture medium for enterobacteria. *J. Bacteriol.* **119,** 736–747 Medline
55. Bertani, G. (1951) Studies on lysogenesis. I. The mode of phage liberation by lysogenic *Escherichia coli*. *J. Bacteriol.* **62,** 293–300 Medline
56. Nelson, C. E., Beri, N. R., and Gardner, J. G. (2016) Custom fabrication of biomass containment devices using 3-D printing enables bacterial growth analyses with complex insoluble substrates. *J. Microbiol. Methods* **130,** 136–143 CrossRef Medline
57. Schäfer, A., Tauch, A., Jäger, W., Kalinowski, J., Thierbach, G., and Pühler, A. (1994) Small mobilizable multi-purpose cloning vectors derived from the *Escherichia coli* plasmids pK18 and pK19: selection of defined deletions in the chromosome of *Corynebacterium glutamicum*. *Gene* **145,** 69–73 CrossRef Medline
58. Gibson, D. G., Young, L., Chuang, R. Y., Venter, J. C., Hutchison, C. A., 3rd, and Smith, H. O. (2009) Enzymatic assembly of DNA molecules up to several hundred kilobases. *Nature Methods* **6,** 343–345 CrossRef Medline
59. Figurski, D. H., and Helinski, D. R. (1979) Replication of an origin-containing derivative of plasmid RK2 dependent on a plasmid function provided in trans. *Proc. Natl. Acad. Sci. U.S.A.* **76,** 1648–1652 CrossRef Medline
60. Murthy, N. K. S., and Bleakley, B. H. (2017) Simplified method of preparing colloidal chitin used for screening of chitinase-producing microorganisms. *Internet J. Microbiol.* **10,** http://ispub.com/IJMB/10/2/14186
61. Janson, G., Zhang, C., Prado, M. G., and Paiardini, A. (2017) PyMod 2.0: improvements in protein sequence-structure analysis and homology modeling within PyMOL. *Bioinformatics* **33,** 444–446 Medline
62. Savitsky, P., Bray, J., Cooper, C. D., Marsden, B. D., Mahajan, P., Burgess-Brown, N. A., and Gileadi, O. (2010) High-throughput production of human proteins for crystallization: the SGC experience. *J. Struct. Biol.* **172,** 3–13 CrossRef Medline
63. Aslanidis, C., and de Jong, P. J. (1990) Ligation-independent cloning of PCR products (LIC-PCR). *Nucleic Acids Res.* **18,** 6069–6074 CrossRef Medline
64. Mekasha, S., Byman, I. R., Lynch, C., Toupalova, H., Andera, L., Naes, T., Vaaje-Kolstad, G., and Eijsink, V. G. H. (2017) Development of enzyme cocktails for complete saccharification of chitin using monocomponent enzymes from *Serratia marcescens*. *Process Biochem.* **56,** 132–138 CrossRef
65. Liu, W., Xie, Y., Ma, J., Luo, X., Nie, P., Zuo, Z., Lahrmann, U., Zhao, Q., Zheng, Y., Zhao, Y., Xue, Y., and Ren, J. (2015) IBS: an illustrator for the presentation and visualization of biological sequences. *Bioinformatics* **31,** 3359–3361 CrossRef Medline